Supplemental Materials of **"Coexistence and interaction of spinons and magnons in an antiferromagnet with alternating antiferromagnetic and ferromagnetic quantum spin chains"**

H. Zhang[1], Z. Zhao[2], D. Gautreau[3], M. Raczkowski[4], A. Saha[3], V.O. Garlea[5], H. Cao[5], T. Hong[5], H. O. Jeschke[6], Subhendra D. Mahanti[1], T. Birol[3], F. F. Assaad[4], X. Ke[1]

I. Experimental methods

Single crystals of Botallackite $Cu_2(OH)_3Br$ samples were synthesized using a conventional hydrothermal method which was detailed in an earlier report [1]. This material crystalizes in the monoclinic space group $P2_1/m$ (No. 11) with lattice constants a = 5.661 Å, b = 6.160 Å, c = 6.083 Å and crystal angles $\alpha = \gamma = 90°, \beta = 93.6°$ at room temperature [1,2]. Magnetization and specific heat were measured using a SQUID magnetometer and a Physical Property Measurement System (Quantum Design) respectively. Neutron diffraction experiments were performed using the HB-3A four-circle diffractometer (λ = 1.5426 Å) at High Flux Isotope Reactor (HFIR) in Oak Ridge National Laboratory (ORNL). Inelastic neutron scattering measurements were conducted on the HYSPEC time-of-flight spectrometer at Spallation Neutron Source (SNS) in ORNL. The incident neutron energy was fixed at E_i = 15 meV. The samples were oriented in the (H K 0) scattering plane, where (H K L) are in units of reciprocal lattice vectors $2\pi/a$, $2\pi/b$, and $2\pi/c$. Co-aligned samples of ~ 1.2 grams were top-loaded into a closed-cycle refrigerator. A total of 151 rocking scans were measured with samples rotated about the c-axis over 150° with 1° step size. The measurements were performed at T = 5 K and 100 K, with the latter data used for background subtraction from the lower temperature data. We followed the detailed procedures reported in Ref. [3] to subtract both temperature-independent background and phonon

scattering background in order to obtain the intrinsic magnetic inelastic scattering signal.

II. Rietveld refinement of single crystal neutron diffraction data on $Cu_2(OH)_3Br$

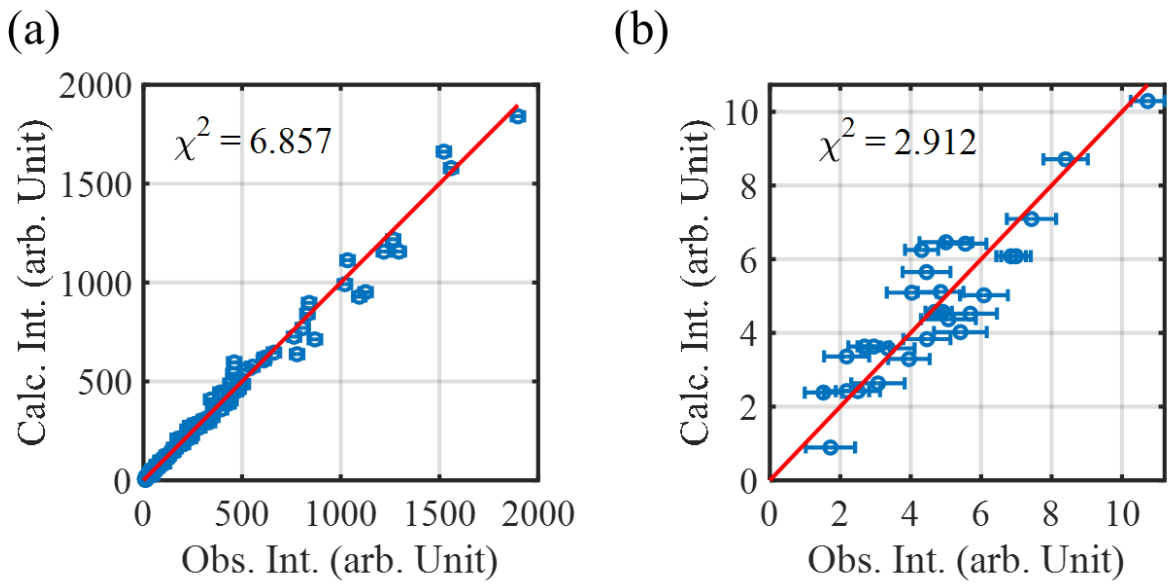

Figure S1 Plots of the comparison of observed and calculated intensities via Rietveld refinement of various (a) nuclear and (b) magnetic diffraction peaks measured at T = 4.6 K. Red lines are visual guides.

III. Linear Spin Wave fitting

By performing linear spin wave (LSW) fitting to the measured inelastic neutron scattering spectra using SpinW [4], we aim to have a preliminary understanding of the spin dynamics of $Cu_2(OH)_3Br$ and extract the parameters of the spin Hamiltonian. **1)** Considering that the magnetic excitation exhibits nearly dispersionless features along both H and L directions (Fig. 2a&b), we first tried to estimate the appropriate intra-chain couplings J_1, J_2 while setting the inter-chain couplings J_3 and J_4 to be zero. In Fig. S2(a), we show the simulation result with J_1 = -2.6 meV and J_2 = 9.9 meV. As expected, both magnon dispersions are gapless. One can see that the calculated magnon dispersion associated with the ferromagnetic chain nearly captures the experimental data

with similar bandwidth, while the bandwidth of the calculated magnon dispersion for the antiferromagnetic chain is larger than the experimental observations. **2)** To account for the gapped behavior, the continuous spin rotational symmetry needs to be broken. For a quantum spin-1/2 system, we considered a Heisenberg-Ising type exchange anisotropy (XXZ). Note that strong magnetic anisotropy behavior has been observed in magnetic susceptibility measurements [1]. Figure S2(b) presents the simulation results using an XXZ type Hamiltonian,

$$H = \sum_{ij} J_{ij}\left[S_i^x S_j^x + S_i^y S_j^y + \left(1 + \Delta_{AF,F}\right) S_i^z S_j^z\right], \Delta_{\mathrm{AF}} = 0.045, \Delta_F = 0.173;$$

A small exchange anisotropy Δ is sufficient to open a large gap at the zone center of the antiferromagnetic branch. **3)** In order to account for the gaps near K = -0.5 and -1.5 observed in the ferromagnetic branch (Fig. 2c), we need to include the next-nearest-neighbor Dzyaloshinskii–Moriya (DM) interaction (D = 1 meV) (between neighboring ferromagnetic and antiferromagnetic spin chains) in the Hamiltonian. Figure S2(c) presents the simulation results with the DM interaction included, which agrees well with the experimental data shown in Fig. 2(c). **4)** As the system exhibits long-range order, one also needs to take into account the inter-chain couplings J_3 and J_4, even though they are relatively weak. The molecular field arising from the ferromagnetic (antiferromagnetic) chains can induce a gap in the magnetic excitation of the neighboring antiferromagnetic (ferromagnetic) chains. This is particularly true for the magnetic excitation of antiferromagnetic chains, which is further supported by the quantum Monte Carlo simulation as shown in Fig. 4. The LSW simulation result with the full set of parameters described in the main text is shown in Fig. 2(d) and its comparison with the experimental data is presented in Fig. 2(c).

It is worth noting that, although it is difficult to precisely determine the inter-chain couplings J_3 and J_4 due to the nearly dispersionless excitation along the H direction, the overall

good agreement between the experimental data and the LSW fitting with or without J_3 and J_4 supports the quasi-1D nature of the magnetic coupling between Cu^{2+} ions.

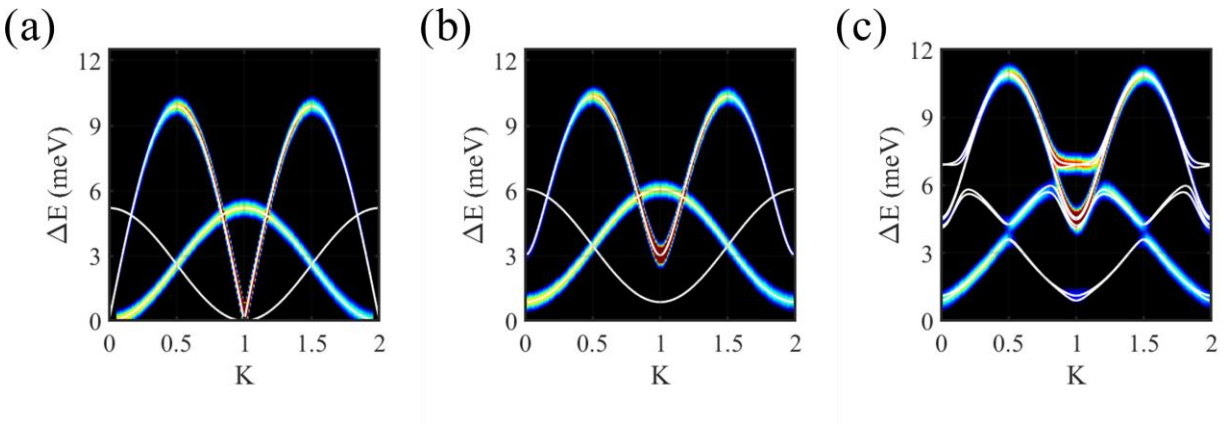

Figure S2 Linear Spin Wave simulation results of different model Hamiltonians. (a) An isotropic Heisenberg model with only intra-chain couplings J_1-J_2. (b) A Heisenberg-Ising (XXZ) model with only intra-chain couplings J_1-J_2. (c) A Heisenberg-Ising model with nearest neighbor intra-chain couplings J_1-J_2 (J_1 = -2.6 meV, J_2 = 9.9 meV), inter-chain coupling (J_3 = 1.2 meV, J_4 = 0.3 meV) and Dzyaloshinskii–Moriya (D = 1 meV) interaction.

IV. Two magnon continuum

To exclude the possibility that the observed continuum is a two-magnon continuum instead of spinon continuum, we calculate the upper- and lower- bounds of the two-magnon continuum. These bounds are defined as the maximum and minimum of the total energy transfer with the momentum transfer conserved [5].

$$\begin{cases} q_t = q_1 + q_2 \\ E_{bound}(q_t) = [\min(E_1 + E_2)\ \max(E_1 + E_2)] \end{cases}$$

In Fig. S3, we show the calculated two-magnon spectra bounds, which are plotted together with the experimental data. The white and red dashed lines indicate the lower and upper bounds respectively. Spectra bounds for two-magnons from the magnetic excitation of ferromagnetic chains, antiferromagnetic chains, and ferromagnetic-antiferromagnetic chains are presented in Fig. S3(a), Fig. S3(b) and Fig. S3(c) respectively. It is known that that two-magnon continuum tends

to have large spectral weight near the lower bounds [5,6]. Nevertheless, none of them can account for the continuum observed in the experiment. In contrast, in Fig. S3(d) we plot the spectra bounds calculated using the modified Muller Ansatz (See. Sec. VI). The spectral weight of the Muller Ansatz is larger near its lower boundary [7], which agrees well with our experimental observations. Thus, we conclude that the experimentally observed continuum cannot be associated with a two-magnon process; instead, it should be associated with a typical spinon continuum observed in quasi-1D quantum antiferromagnets with S=1/2.

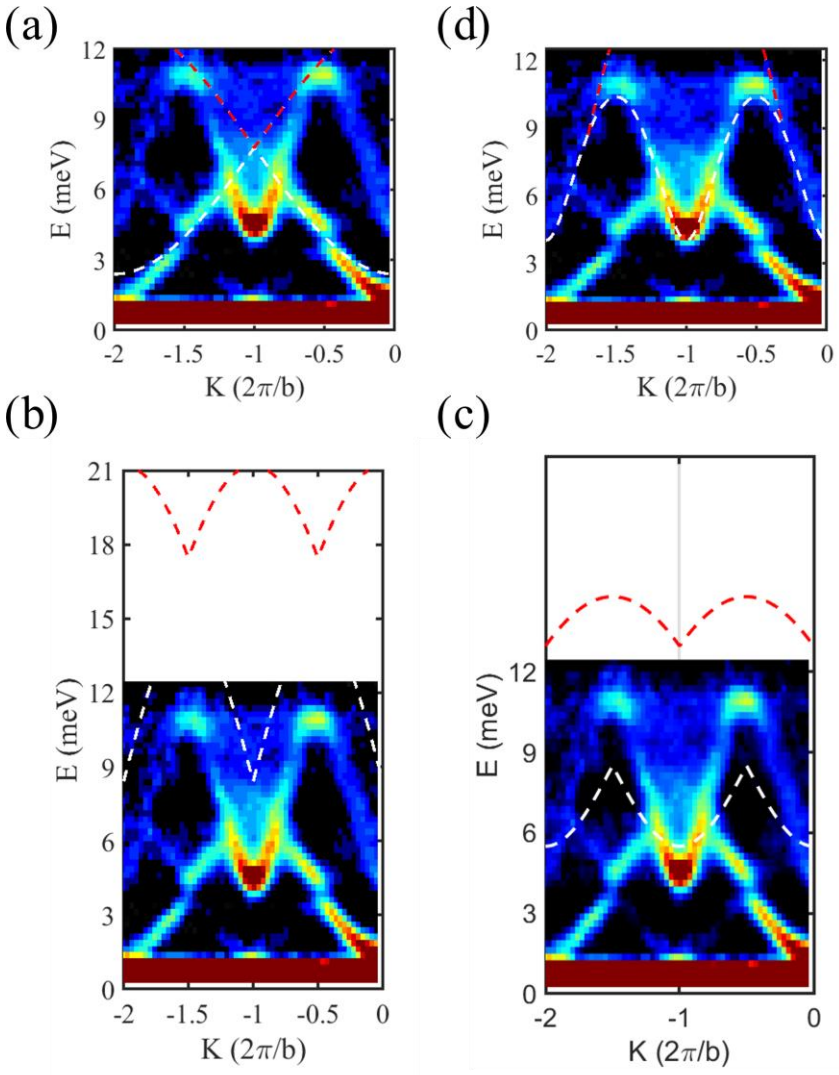

Figure S3 Two-magnon spectra bounds plotted together with experimental data. (a) Spectra bounds of two-magnons for the ferromagnetic branch. (b) Spectra bounds of two-magnons for the

antiferromagnetic branch. (c) Spectra bounds of two-magnons for both ferromagnetic and antiferromagnetic branches. (d) Spectra bounds of the modified Muller Ansatz.

V. Density Functional Theory (DFT) calculation

To understand the atomic and electronic structures and the nature of exchange coupling, density functional theory (DFT) calculations were performed using Projector Augmented Wave method implemented in the Vienna *Ab Initio* Simulation Package (VASP) [8-11]. PBEsol approximation to the exchange correlation functional [12] was used and an 8 x 8 x 8 **k**-point grid was used in the numerical calculations. To properly reproduce the local magnetic moments on Cu^{2+} ions, the rotationally invariant DFT + U scheme with U = 4 eV and J = 0 eV was used. Total energy calculations for several magnetic configurations (Fig. S4) were carried out and used to fit the parameters of an isotropic Heisenberg model. We used a two-dimensional (2D) model with both intra-chain and inter-chain interactions. The 2D model, which ignores interactions between Cu spins belonging to neighboring layers along the c-axis, is reasonable because of the absence of any shared oxygen or bromine bridging ligands between the Cu^{2+} ions on adjacent layers.

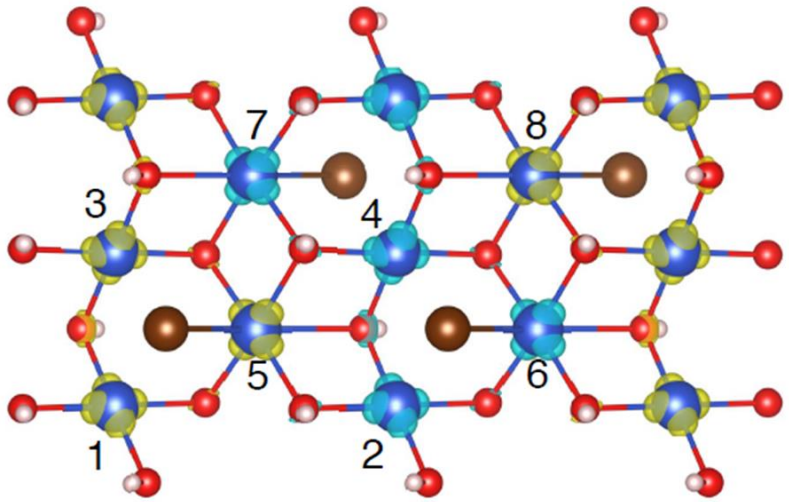

	Configuration	Energy (eV)
1	1 -1 1 -1 -1 1 1 -1	-157.52696
2	1 -1 1 -1 -1 -1 1 1	-157.52930
3	1 1 1 1 -1 -1 -1 -1	-157.50093
4	1 -1 -1 1 -1 1 1 -1	-157.51923
5	1 1 -1 -1 1 1 -1 -1	-157.51972
6	1 -1 1 -1 1 -1 1 -1	-157.49364
7	1 1 1 -1 -1 -1 1 -1	-157.50687
8	1 1 -1 -1 1 -1 1 -1	-157.47824
9	1 1 1 -1 1 -1 -1 -1	-157.50855
10	1 1 1 -1 -1 1 1 1	-157.50183
11	1 1 1 -1 -1 1 1 -1	-157.52309
12	1 1 1 -1 -1 1 -1 1	-157.48585
13	1 1 1 -1 -1 -1 1 1	-157.52423
14	1 1 -1 1 1 1 1 1	-157.48083
15	1 1 -1 1 1 1 1 -1	-157.50335
16	1 1 1 1 1 -1 1 1	-157.50507
17	1 -1 1 -1 1 1 1 -1	-157.50992
18	1 -1 1 -1 1 -1 -1 1	-157.53305
19	1 1 1 1 1 1 1 1	-157.48116

Figure S4 Color-coded electron density profile from Density Function Theory (DFT+U with U = 4 eV) calculations using PBEsol. Spin-up electrons are colored in yellow and spin-down electrons are colored in light-blue. Eight copper ions in the magnetic unit cell are numbered. The spin configuration #18 highlighted in red box of the right table has the lowest energy. This spin configuration is the same as observed by neutron diffraction experiment (Sec. I).

In order to understand the effect of U on the exchange parameters we also performed DFT+U calculations with different values of U and obtained qualitatively similar results. That is, J_1 and J_2 are the most dominant couplings, which lead to ferromagnetic and antiferromagnetic chains of spins; the inter-chain couplings between neighboring ferromagnetic and antiferromagnetic chains, J_3 and J_4, are weak and antiferromagnetic, while further-neighbor inter-chain couplings between neighboring antiferromagnetic chains or between neighboring ferromagnetic chains, J_5 and J_6, are even weaker and negligible, as shown in Fig. S5.

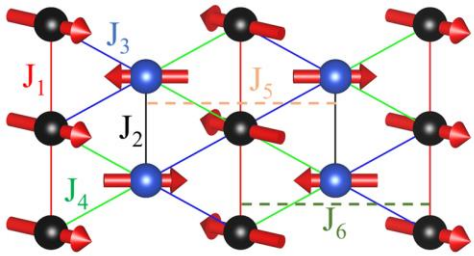

	U = 3 eV	U = 4 eV	U = 5 eV	U = 6 eV
J_1 (meV)	-1.9 ± 0.2	-1.41 ± 0.1	-1.1 ± 0.06	-0.84 ± 0.03
J_2 (meV)	6.1 ± 0.2	4.81 ± 0.09	3.74 ± 0.05	2.84 ± 0.03
J_3 (meV)	1.3 ± 0.1	0.83 ± 0.07	0.5 ± 0.04	0.28 ± 0.02
J_4 (meV)	0.7 ± 0.1	0.42 ± 0.07	0.25 ± 0.04	0.15 ± 0.02
J_5 (meV)	0.3 ± 0.7	0.14 ± 0.09	0.08 ± 0.05	0.05 ± 0.03
J_6 (meV)	0 ± 0.2	-0.01 ± 0.09	0 ± 0.05	0 ± 0.03

Figure S5 DFT calculated exchange interactions (up to J_6) using different U values. Left is an illustration of different exchange interactions (J_s). Note that the relative ratios of J_s values are consistent with our LSW fitting results (See Sec. II) and J_5 and J_6 are much smaller compared to J_1 up to J_4.

In order to check the sensitivity of the exchange parameters to different approximations to the exchange-correlation potential within DFT+U, we performed GGA+U calculations within the full potential local orbital (FPLO) basis [13]. The table shown in Fig. S6 presents the calculated exchange couplings with different U values. This result reaffirms the existence of ferromagnetic and antiferromagnetic chains and it indicates that there are finite antiferromagnetic couplings between the chains. Here we note that in contrast to the results discussed above, the inter-chain coupling between neighboring antiferromagnetic chains J_5 obtained using GGA+U approximation

is relatively large compared to other inter-chain couplings J_3, J_4, and J_6. LSW calculations using these sets of exchange parameters yield qualitatively distinct dispersion features. In addition, the large J_5 would lead to a negative sign problem in quantum Monte Carlo simulations presented below. The discrepancy in J_5 obtained in DFT calculations using GGA+U and PBEsol+U approximations warrants further careful investigation.

	U = 6 eV	U = 7 eV	U = 8 eV	U = 9 eV
J_1 (meV)	-2.86 ± 0.07	-2.41 ± 0.05	-2.10 ± 0.03	-1.89 ± 0.02
J_2 (meV)	13.34 ± 0.07	10.34 ± 0.05	7.76 ± 0.03	5.58 ± 0.02
J_3 (meV)	2.51 ± 0.06	1.76 ± 0.04	1.18 ± 0.03	0.74 ± 0.02
J_4 (meV)	1.18 ± 0.06	1.00 ± 0.04	0.85 ± 0.03	0.70 ± 0.02
J_5 (meV)	1.90 ± 0.05	1.70 ± 0.04	1.50 ± 0.03	1.32 ± 0.02
J_6 (meV)	0.24 ± 0.06	0.13 ± 0.04	0.07 ± 0.03	0.03 ± 0.02

Figure S6 A table listing exchange couplings calculated using DFT with GGA+U approximation. Exchange parameters are calculated with GGA+U as function of interaction strength U and for fixed J_H = 1 eV.

VI. Quantum Monte Carlo (QMC) Simulations

(a) QMC Method

We have used the Algorithms for Lattice Fermions (ALF)-implementation [14] of the finite temperature auxiliary field quantum Monte Carlo [14,15] to carry out the numerical simulations. While this algorithm is formulated for fermionic systems, it can also be used to simulate non-frustrated spin systems. Consider the following sipn-1/2 model on an arbitrary lattice

$$\hat{H} = \sum_{i,j} J_{ij} \vec{S}_i \cdot \vec{S}_j$$

We chose a Fermionic representation of the spin operators, $\vec{S}_i = \frac{1}{2} \hat{f}_i^\dagger \vec{\sigma} \hat{f}_i$ with $\hat{f}_i^\dagger = \left(\hat{f}_{i,\uparrow}^\dagger, \hat{f}_{i,\downarrow}^\dagger\right)$ and constraint $\hat{f}_i^\dagger \hat{f}_i = 1$. The above Hamiltonian can then be rewritten as:

$$\widehat{H}_F = \widehat{H}_J + \widehat{H}_U$$

with $\widehat{H}_J = -\sum_i \frac{J_{ij}}{4} \left(\hat{f}_i^\dagger \hat{f}_j + \hat{f}_j^\dagger \hat{f}_i\right)^2$ and $\widehat{H}_U = \frac{U}{2}\sum_i \left(\hat{f}_i^\dagger \hat{f}_i - 1\right)^2$

In the limit $U \to \infty$, the constraint $\hat{f}_i^\dagger \hat{f}_i = 1$ becomes exact, and $\widehat{H}_F$ reduces to the desired Hamiltonian $\widehat{H}$. Importantly, $\left[\widehat{H}_U, \widehat{H}_J\right] = 0$ so that the constraint is very efficiently imposed. In fact, in our simulations the double occupancy takes the value $\langle \hat{f}_{i,\uparrow}^\dagger \hat{f}_{i,\uparrow} \hat{f}_{i,\downarrow}^\dagger \hat{f}_{i,\downarrow} \rangle = 0.000145 \pm 0.0002$ for the choice U/J_2 =1 and $\beta J_2 = 20$. J_2 is the intra-chain coupling of the antiferromagnetic chains. The fermionic Hamiltonian is written in terms of a sum of perfect squares and complies with the standard of the ALF-library so that it is straightforward to implement it [14]. The absence of negative sign problem follows from particle-hole symmetry and the following restriction for the choice of the couplings. Assume that it is possible to find a bipartition of the graph into two subgraphs, A and B. Provided that the magnetic coupling between A and B is antiferromagnetic and that it is ferromagnetic between lattice sites within the same graph, then one can demonstrate the absence of negative sign problem. To carry out the Wick rotation from imaginary to real time, we use the stochastic maximum entropy [16] implementation of the ALF-library. We have taken into account the covariance matrix and produced high quality data with relative error below 0.5%. For the runs we have used an imaginary time step of $\Delta\tau J_2 = 0.1$.

(b) **Calculation of dynamical spin structure factor**

Let $\boldsymbol{R}$ denote the unit cell and α the Cu^{2+} position in the unit cell. The position of Cu^{2+} ion reads $\boldsymbol{R} + \boldsymbol{r}_\alpha$. $r_1 = (0,0), r_2 = (0.5,0), r_3 = (0.25,0.5), r_4 = (0.75,.50)$. Each orbital accommodates a spin-1/2 degree of freedom, $\hat{S}_\alpha(\boldsymbol{R})$. Consider

$$\widehat{N}_\alpha(\boldsymbol{q}) = \frac{1}{\sqrt{N}} \sum_{R,\beta} e^{i\boldsymbol{q}\cdot(\boldsymbol{R}+\boldsymbol{r}_\beta)} U_{\alpha,\beta} \hat{S}_\beta(\boldsymbol{R})$$

and the matrix U is yet to be specified. Generally, we can compute

$$S_\alpha(\boldsymbol{q},\tau) = \langle \widehat{N}_\alpha(\boldsymbol{q},\tau) \cdot \widehat{N}_\alpha^\dagger(\boldsymbol{q},0) \rangle$$

and the corresponding spectra function is obtained with analytical continuations:

$$S_\alpha(\boldsymbol{q},\tau) = \frac{1}{\pi} \int d\omega e^{-\tau\omega} S_\alpha(\boldsymbol{q},\omega) = \frac{1}{\pi} \int d\omega \frac{e^{-\tau\omega}}{1-e^{-\beta\omega}} \chi''_\alpha(q,\omega)$$

To best capture the physics of our system, we will consider three quantities

$$\frac{1}{N_\alpha} \sum_\alpha S_\alpha(\mathbf{q},\tau) = S^{tot}(\mathbf{q},\tau)$$

with arbitrary unitary matrix, $UU^\dagger = 1$.

For the antiferromagnetic spin chains, $\widehat{N}_{AF}(\boldsymbol{q}=(2\pi,K)) = \frac{1}{\sqrt{2L_x}} \sum_{R_x,\beta=1,2} e^{i\boldsymbol{q}\cdot(\boldsymbol{R}+\boldsymbol{r}_\beta)} \hat{S}_\beta$;

For the ferromagnetic spin chains, $\widehat{N}_F(\boldsymbol{q}=(2\pi,K)) = \frac{1}{\sqrt{2L_x}} \sum_{R_x,\beta=3,4} e^{i\boldsymbol{q}\cdot(\boldsymbol{R}+\boldsymbol{r}_\beta)} \hat{S}_\beta$;

Finally, the dynamical spin structure factor in the extended zone scheme is obtained by considering $\widehat{N}_E(\boldsymbol{q}=(2\pi,K)) = \frac{1}{\sqrt{4N}} \sum_{R,\beta=1\ldots4} e^{i\boldsymbol{q}\cdot(\boldsymbol{R}+\boldsymbol{r}_\beta)} \hat{S}_\beta$.

(c) **Magnon Line width of ferromagnetic quantum spin chains**

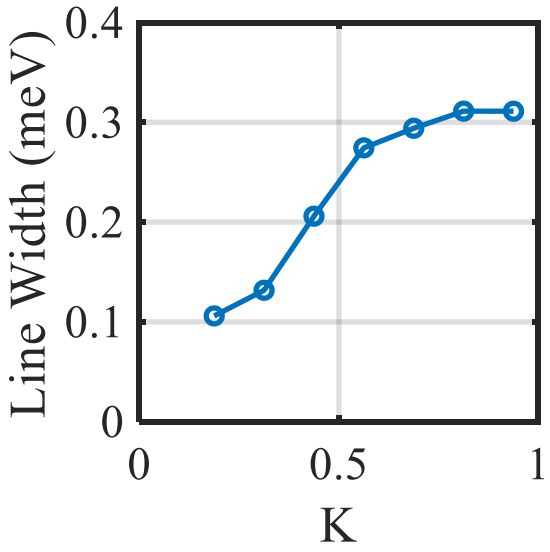

Figure S7 Magnon line width of ferromagnetic quantum spin chains. The line width at each K point is obtained by fitting the I(E) spectra of ferromagnetic chains obtained via QMC simulation using a Lorentzian fit. The inter-chain interaction between ferromagnetic chain and neighboring antiferromagnetic chains is $0.2J_2$. Broader magnon line width is observed near the zone boundary (K = 1).

VI. Random Phase Approximation (RPA) Calculations

The Hamiltonian of interacting spin chains is written as

$$H = H_1 + H_{int}$$

where the intra-chain interaction H_1

$$H_1 = \sum_{\vec{k}} J_1(\vec{k}) \vec{S}_{\vec{k}}^{(F)} \cdot \vec{S}_{-\vec{k}}^{(F)} + \sum_{\vec{k}} J_2(\vec{k}) \vec{S}_{\vec{k}}^{(AF)} \cdot \vec{S}_{-\vec{k}}^{(AF)}$$

with $J_1(\vec{k}) = 2J_1 \cos(\frac{k_y b}{2})$ and $J_2(\vec{k}) = 2J_2 \cos(\frac{k_y b}{2})$. For our system $J_1 < 0$, ferromagnetic and $J_2 > 0$, antiferromagnetic.

And the inter-chain interaction H_{int}

$$H_{int} = \sum_{\vec{k}} J_{\perp}(\vec{k})\, \vec{S}_{\vec{k}}^{(F)} \cdot \vec{S}_{-k}^{(AF)}$$

with $J_{\perp}(\vec{k}) = 4(J_4 + J_3)\cos\left(\frac{k_x a}{2}\right)\cos(\frac{k_y b}{4})$

In order to calculate dynamic susceptibility in RPA, denoted as $\chi_{RPA}^{F,AF}(\vec{k},\omega)$, we apply an external field (space and time dependent) $\vec{H}_{ext}(\vec{k},\omega)$. The total Hamiltonian becomes (we have taken $g\mu_B = 1$).

$$H = H_1 + H_{int} - \sum_{k} \vec{H}_{ext}(\vec{k},\omega).\left(\vec{S}_{\vec{k}}^{(F)} + \vec{S}_{\vec{k}}^{(AF)}\right)$$

First, we define the dynamic susceptibilities (isotropic in spin space) of non-interacting ferromagnetic and antiferromagnetic chains:

$\langle S_{\vec{k}}^{(F)}\rangle = \chi_{1D}^{F}(\vec{k},\omega)H_{ext}(\vec{k},\omega)$;

$$\langle S_{\vec{k}}^{(AF)}\rangle = \chi_{1D}^{AF}(\vec{k},\omega)H_{ext}(\vec{k},\omega)$$

Since the chains are one-dimensional, $\chi_{1D}^{F,AF}(\vec{k},\omega)$ depend only on the component of $\vec{k}$ along the chain direction ($k_{\parallel} \equiv k_y$), $\chi_{1D}^{F,AF}(k_{\parallel},\omega)$. Next, we introduce the coupling between ferromagnetic and antiferromagnetic chains through an effective field approximation.

$\langle S_{\vec{k}}^{(F)}\rangle = \chi_{1D}^{F}(k_{\parallel},\omega)\left[H_{ext}(\vec{k},\omega) - J_{\perp}(k_{\perp})\langle S_{\vec{k}}^{(AF)}\rangle\right]$;

$$\langle S_{\vec{k}}^{(AF)}\rangle = \chi_{1D}^{AF}(k_{\parallel},\omega)\left[H_{ext}(\vec{k},\omega) - J_{\perp}(k_{\perp})\langle S_{\vec{k}}^{(F)}\rangle\right]$$

Solving for $\langle S_{\vec{k}}^{(F)}\rangle$ and $\langle S_{\vec{k}}^{(AF)}\rangle$ and defining $\chi_{RPA}^{F,AF}(\vec{k},\omega)$ as

$$\langle S_{\vec{k}}^{(F,AF)}\rangle = \chi_{RPA}^{F,AF}(\vec{k},\omega)H_{ext}(\vec{k},\omega)$$

We get

$$\chi_{RPA}^{F,AF}(\vec{k},\omega)=\frac{\left[1-J_{\perp}(k_{\perp})\chi_{1D}^{AF,F}(k_{\parallel},\omega)\right]\chi_{1D}^{F,AF}(k_{\parallel},\omega)}{1-[J_{\perp}(k_{\perp})]^{2}\,\chi_{1D}^{AF}(k_{\parallel},\omega)\chi_{1D}^{F}(k_{\parallel},\omega)}$$

For $\chi_{1D}^{F}(k_{\parallel},\omega)$ of ferromagnetic chains, we use a Lorentz function

$$\chi_{1D}{}^{F}(\vec{k},\omega)=\chi_{1D}{}^{F}(k_{\parallel},\omega)=\frac{1}{(\omega-\omega_{F}(k_{\parallel})-i\Gamma)}$$

with $\omega_{F}(k_{\parallel})=2|J_{1}|\left[1-\cos(\frac{k_{\parallel}b}{2})\right]$ and Γ is the line width.

For $\chi_{1D}^{AF}(k_{\parallel},\omega)$ of antiferromagnetic chains, we use

$$\chi_{1D}^{AF}(k_{\parallel},\omega)=\chi_{1D}^{'AF}(k_{\parallel},\omega)+i\chi_{1D}^{''AF}(k_{\parallel},\omega)$$

where $\chi_{1D}^{'AF}(k_{\parallel},\omega)=\int_{0}^{\infty}d\omega'\,S_{1D}^{AF}(k_{\parallel},\omega')/(\omega'-\omega)$ and $\chi_{1D}^{''AF}(k_{\parallel},\omega)=\pi*S_{1D}^{AF}(k_{\parallel},\omega)$.

$$S_{1D}^{AF}(k_{\parallel},\omega)=\frac{C\theta(\omega-\omega_{l}(k_{\parallel}))\theta(\omega_{u}(k_{\parallel})-\omega)}{\sqrt{\omega^{2}-\omega_{l}^{2}(k_{\parallel})}}$$

$$\omega_{u}^{2}=\left(\pi J_{2}*\sin(k_{||}b/4)\right)^{2}$$

$$\omega_{l}^{2}=\sqrt{\Delta_{g}^{2}+\left(\frac{\pi J_{2}*\sin(k_{||}b/2)}{2}\right)^{2}},\Delta_{g}=4.0meV$$

Here C is a constant, θ is the Heaviside step function, and ω_{l} and ω_{u} are the lower and upper energy boundaries of the two-spinon continuum. A nominal value of the spin gap Δ_{g} is included in the expression of ω_{l}. The exchange interactions are: J_1 = -2.7 meV, J_2 = 6.1 meV and $J_3 + J_4$ = 0.6 meV. Note that here J_2 value is (2/π) times of that obtained from the LSW fitting. This is due to the difference in pre-factor for LSW theory and Muller Ansatz. For simplicity, we set D = 0 in

the calculations and introduce nominal gap values in the excitation spectrum to account for the effect of Δ and the static mean field due to inter-chain couplings

The total spectrum intensity is written as the product of Bose factor (n_B), magnetic form factor ($f.f.$) and generalized susceptibility (χ),

$$I_{RPA}(\vec{k},\omega) = \frac{\left(\chi''^{F}_{RPA}(\vec{k},\omega) + \chi''^{AF}_{RPA}(\vec{k},\omega)\right)}{\pi} \cdot n_{Bose} \cdot f.f._{(Cu^{2+})}$$

In addition to the comparison of constant E cuts obtained from the experimental and RPA calculation results presented in Fig. 5 in the main text, we also perform constant K cuts and compare the results as shown in Fig. S8(a, b). For K = -1.45 we see peaks associated with both the magnons (~ 4.5 meV) and lower edge of the spinon continuum (~ 11 meV). RPA with an inter-chain coupling reproduces the entire spectrum well. The small discrepancy in the magnon dispersion is due to the neglect of the D term in the RPA calculations. The D term opens a gap in the magnon dispersion and shifts the upper branch upwards (Fig. 2(c, d) and Fig. 5(a)). The experimental line shapes are also reproduced well within RPA. For K = -1 (i.e., $k_{\parallel} = -2\pi/b$), $J_{\perp}(K) = 0$ and RPA reduces to dynamically decoupled F and AF chains. The lower energy peak associated with the AF chain agrees reasonably well with theory but the high energy magnon peak does not. One cannot ascribe this disagreement to RPA because $J_{\perp}(K) = 0$. We suggest that the single well-defined magnon excitation picture used in the RPA calculation for isolated 1D S = 1/2 ferromagnetic chains is not adequate. One has to incorporate a temperature and momentum dependent magnon line width. Magnon-magnon interactions in quantum S = 1/2 ferromagnetic spin chains and thermal fluctuations are important and have to be incorporated into the theory. In fact, strong experimental evidence of large spin-wave line width at temperatures $k_B T\ /|J_1| \sim 0.1 - 0.2$, particularly for zone boundary magnons was reported by Satija et al in 1D S = 1/2 Heisenberg

ferromagnet $CuCl_2$-DMSO [17]. It was pointed out that the magnitude and q-dependence of the line width obtained from theoretical calculations using semi-classical spins [18] were inadequate to explain the measurements and the explicit quantum nature of the spins had to be considered [17]. Indeed, broadened magnon line width of the ferromagnetic chains near the zone boundary is confirmed in quantum Monte Carlo simulation, as shown in Fig. S7.

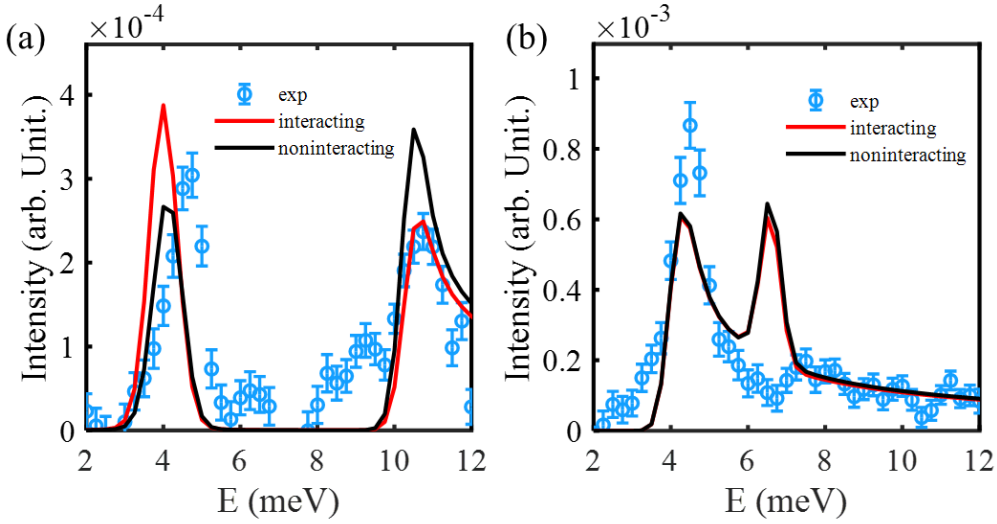

Figure S8 Magnetic excitation spectra and comparison with RPA calculations. Constant Q cuts at K = -1.45 (a) and K = -1 (b) and comparison with RPA calculations. Red and black correspond to with and without inter-chain interactions.

References

[1] Z. Y. Zhao, H. L. Che, R. Chen, J. F. Wang, X. F. Sun, and Z. Z. He, J Phys-Condens Mat **31** (2019).

[2] X. G. Zheng, T. Yamashita, M. Hagihala, M. Fujihala, and T. Kawae, Physica B: Condensed Matter **404**, 680 (2009).

[3] T. Hong *et al.*, Physical Review B **74**, 094434 (2006).

[4] S. Toth and B. Lake, Journal of Physics: Condensed Matter **27**, 166002 (2015).

[5] M. B. Stone, I. A. Zaliznyak, T. Hong, C. L. Broholm, and D. H. Reich, Nature **440**, 187 (2006).

[6] T. Huberman, R. Coldea, R. A. Cowley, D. A. Tennant, R. L. Leheny, R. J. Christianson, and C. D. Frost, Physical Review B **72**, 014413 (2005).

[7] M. Karbach, G. Müller, A. H. Bougourzi, A. Fledderjohann, and K.-H. Mütter, Physical Review B **55**, 12510 (1997).

[8] G. Kresse and J. Furthmüller, Physical Review B **54**, 11169 (1996).
[9] S. L. Dudarev, G. A. Botton, S. Y. Savrasov, C. J. Humphreys, and A. P. Sutton, Physical Review B **57**, 1505 (1998).
[10] G. Kresse and J. Hafner, Physical Review B **47**, 558 (1993).
[11] G. Kresse and D. Joubert, Physical Review B **59**, 1758 (1999).
[12] J. P. Perdew, K. Burke, and M. Ernzerhof, Physical Review Letters **77**, 3865 (1996).
[13] K. Koepernik and H. Eschrig, Physical Review B **59**, 1743 (1999).
[14] M. Bercx, F. Goth, J. S. Hofmann, and F. F. Assaad, SciPost Phys. **3**, 013 (2017).
[15] F. Assaad and H. Evertz, *Computational Many-Particle Physics* (Springer-Verlag, Berlin, 2008), Vol. 739, Lecture Notes in Physics, p.^pp. 277-356.
[16] A. W. Sandvik, Physical Review B **57**, 10287 (1998).
[17] S. K. Satija, J. D. Axe, R. Gaura, R. Willett, and C. P. Landee, Physical Review B **25**, 6855 (1982).
[18] G. Reiter and A. Sjolander, Journal of Physics C: Solid State Physics **13**, 3027 (1980).